PCCP

Accepted Manuscript

ROYAL SOCIETY OF CHEMISTRY

www.rsc.org/pccp

Graphical Abstract

Symmetry breaking in the planar configurations of disilicontetrahalides. Correlations between the Pseudo Jahn-Teller effect parameters, hardness and electronegativity

Ghazaleh Kouchakzadeh and Davood Nori-Shargh*

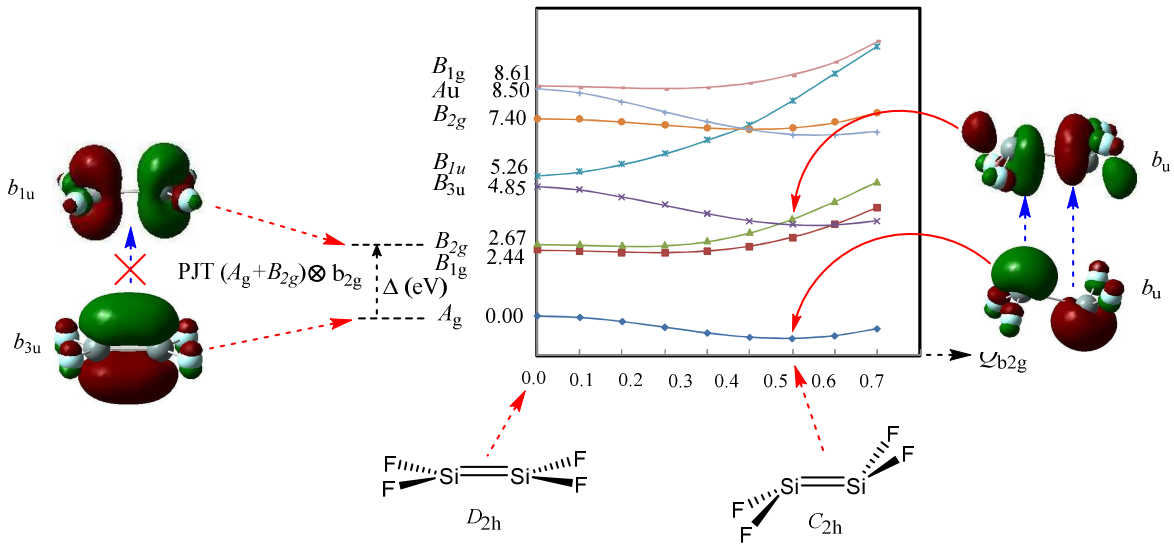

Symmetry breaking in the planar configurations of disilicontetrahalides. Correlations between the Pseudo Jahn-Teller effect parameters, hardness and electronegativity

Ghazaleh Kouchakzadeh and Davood Nori-Shargh*

Department of Chemistry, Arak Branch, Islamic Azad University, Arak, Iran

Abstract:

CCSD(T), MP2, LC-BLYP, LC-ωPBE and B3LYP methods with the Def2-TZVPP basis set and natural bond orbital (NBO) interpretations were performed to investigate the correlations between the Pseudo-Jahn-Teller Effect (*PJTE*) parameters [*i.e.* vibronic coupling constant values (F), energy gaps between reference states (Δ) and primary force constant (K_0)], structural and configurational properties, global hardness, global electronegativity, natural bond orders, stabilization energies associated with the electron delocalizations and natural atomic charges of disilicontetrafluoride (**1**), disilicontetrachloride (**2**), disilicontetrabromide (**3**) and disilicontetraiodide (**4**). All levels of theory showed the *trans*-bent (C_{2h}) configurations as the energy minimum structures of compounds **1-4** and the flap angles between the X_2Si planes and the Si=Si bonds in the distorted (C_{2h}) configurations decrease from compound **1** to compound **4**. The negative curvatures of the ground state electronic configurations and the positive curvatures of the excited states of the *adiabatic potential energy surfaces* (*APESs*) which are resulted from mixing of the ground A_g and excited B_{2g} states are due to the *PJTE* (i.e. *PJT* $(A_g + B_{2g}) \otimes b_{2g}$ problem). Contrary to usual expectation, with the decrease of the energy gaps between reference states (Δ), the *PJTE* stabilization energy, E_{PJT}, decrease from compound **1** to compound **4**. The canonical molecular orbital (CMO) analysis revealed that the contributions of the $\psi_{HOMO}(b_{3u})$ and $\psi_{LUMO}(b_{1u})$ molecular orbitals in the vibronic coupling constant (F) decrease from compound **1** to compound **4**. This fact clearly justifies the decrease of the vibronic coupling constant (F) and primary force constant (the force constant without the *PJTE*) values ongoing from compound **1** to compound **4**, leading to the decrease of the negative curvatures of the ground state electronic configuration curves of their corresponding *APESs*. The results obtained showed that the stabilization energies associated with the mixing of the distorted donor $\pi_{si\text{-}si}(b_u)$ bonding and acceptor $\sigma^*_{si\text{-}si}(b_u)$

antibonding orbitals along the b_{2g} bending distortions decreases from compound **1** to compound **4**. This fact reasonably explains the increase of the Si-Si natural bond orders (*nbo*) ongoing from compound **1** to compound **4**. With the increase of the Si-Si natural bond orders, the corresponding E_{PJT} decrease form compound **1** to compound **4**. Importantly, the variations of the global hardness (η) differences ($\Delta[\eta(C_{2h})-\eta(D_{2h})]$) do not correlate with the trend observed for their corresponding total energy differences, justifying that the configurational properties of compounds **1-4** do not obey the *maximum hardness principle*. Interestingly, the *trans*-bent (C_{2h}) configurations of compounds **1-4** are more electronegative than their corresponding planar (D_{2h}) forms and the variations of their global electronegativity (χ) differences ($\Delta[\chi(C_{2h})-\chi(D_{2h})]$) succeed in accounting for the decrease of the E_{PJT} stabilization energies for the $D_{2h}\rightarrow C_{2h}$ conversion processes ongoing from compound **1** to compound **4**.

Keywords: pseudo Jahn-Teller effect, disilicontetrahalides, canonical molecular orbital, symmetry breaking

*Corresponding authors: E-mail address: nori_ir@yahoo.com

Introduction

Ethene has a planar structure but the results obtained from theoretical calculations[1-18] and experiments (e.g. X-ray,[19-22]) have been demonstrated a *trans*-bent structure for disilene derivatives (as a heavier analog of ethene).

The geometries of the substituted disilene is strongly dependent on the electronagativity of their substituents.[23-26] In 1990, Karni and Apeloig pointed out that disilenes with electronegative and π-bonding substituents are largely deviated from planarity but the electropositive substituents have opposite impacts.[27]

Recently, Mondal and co-workers prepared the Si_2Cl_4 species (with *trans*-bent structure) which was stabilized as singlet biradical utilizing two cyclic alkyl(amino) carbene substituents which is stable, isolable, and storable at room temperature under an inert atmosphere.[28]

Although there are sufficient information in the literature about the structural properties of the substituted disilenes, there are no published data concerning the origin of the substituents impacts on the planarity and *trans*-bending of disilene derivatives. It is now timely to investigate the origin of the symmetry breaking in the planar configurations of disilene derivatives.

It is well known that the Jahn-Teller (*JT*) effect (*JTE*) (including the proper *JTE* for systems in electronically degenerate states, the Renner-Teller effect (*RTE*) for linear molecules, and pseudo *JTE* (*PJTE*) for any system) is only source of structural distortions of high-symmetry configurations of any molecular system.[29-32]

Symmetry breaking in the high-symmetric configuration of a molecule can results from mixing of the ground and excited electronic states.[29-38] In a two-level problem, the ground and excited electronic states of a given nuclear configuration are well defined and mutual orthogonal, therefore, there is no mixing between the ground and excited electronic states. Under nuclear displacements (Q), the ground and excited electronic states will not be orthogonal; therefore, they may become mixed. This mixing depends on the electronic wavefunctions of the ground ψ_1 and excited ψ_2 states. Also, the symmetry of the concerted (symmetrized) nuclear displacements Q plays a determinant role here. The primary force constant (the force constant without the *PJTE*, K_0) of the ground state in the Q direction for any polyatomic system in the high-symmetry configuration is defined as:

$$K_0 = \left\langle \psi_1 \left| \left(\frac{\partial^2 H}{\partial Q^2}\right)_0 \right| \psi_1 \right\rangle \qquad \text{(eq. 1)}$$

where H is the Hamiltonian. It should be noted that the force constant without the *PJTE* is positive, $K_0 > 0$.[30-32] Under nuclear displacements (Q) and by mixing of the ground state with the excited state, it can be easily shown that the force constant is reduced to $K = K_0 - (F^2/\Delta)$, where F is the vibronic coupling constant,

$$F = \left\langle \psi_1 \left| \left(\frac{\partial H}{\partial Q}\right)_0 \right| \psi_2 \right\rangle \quad \text{(eq. 2)}$$

and Δ is the energy gap between the two reference states. If

$$\frac{F^2}{\Delta} > K_0 \qquad \text{(eq. 3)}$$

$K < 0$, and the system is unstable in the Q direction. By analyzing the symmetries of the wavefunctions of the excited states, following the selection rules for the matrix element (eq. 2) and estimating the values of the three parameters F, Δ, and K_0 in Eq. (eq. 3), we can predict the expected distortion Q. By analogy with the *JTE* this is called *PJTE*. In the multilevel problems, many excited states contribute to K and their effects are summed up.[30-32]

In this work, we have investigated the correlations between the *PJT* parameters [vibronic coupling constant values (F), energy gaps between reference states (Δ) and primary force constant (K_0)], structural and configurational properties, global hardness, global electronegativity and natural charges of disilicontetrafluoride (**1**), disilicontetrachloride (**2**), disilicontetrabromide (**3**) and disilicontetraiodide (**4**) be means of TD-DFT[39] (B3LYP/Def2-TZVPP)[40,41] calculations and natural bond orbital interpretations. The high-symmetric (D_{2h}]) configurations of compounds **1**-**4** can be distorted due to the vibronic coupling (i.e. *PJTE*) by mixing the electronic wavefunctions of the ground and excited states under the $D_{2h} \rightarrow C_{2h}$ distortions. Also, the energy curves of the ground A_g and excited states (e.g. B_{2g}, B_{1g}, B_{3u}, and B_{1u} symmetries) in the distortion

directions of compounds **1-4** were investigated by means of TD-DFT (B3LYP/Def2-TZVPP) calculations.

In addition, the planar (D_{2h}) and *trans*-bent (C_{2h}) geometries of compounds **1-4** have been optimized at the singles and doubles coupled cluster theory corrected with perturbative triples correction [CCSD(T)],[42] second-order Møller-Plesset perturbation theory (MP2),[43,44] the long-range corrected density functional theories (LC-BLYP,[45] LC-ωPBE[46]) and B3LYP[40] methods with Def2-TZVPP[41] basis set on all atoms (scheme 1). Further, the correlations between the *PJT* stabilization energies, stabilization energies associated with the electron delocalizations, orbital occupancies, natural charges, hardness, electronegativity and structural parameters have been investigated

Also, we have used a natural bond orbital (NBO)[47] interpretation to explain the mixing between the M-M π bonding b_u orbitals and M-M σ anti-bonding b_u orbitals in the *trans*-bent structures of compounds **1-4**.

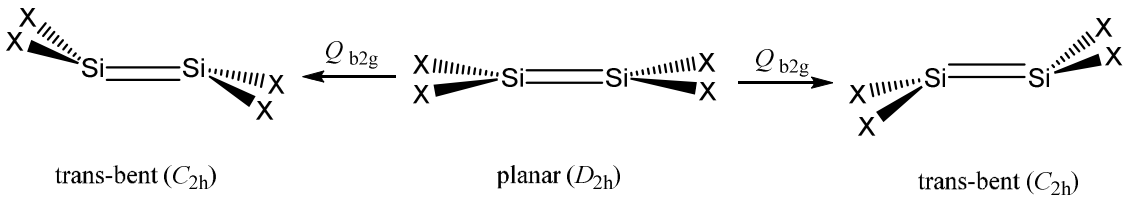

1: X=F, **2**: X=Cl, **3**: X=Br, **4**: X=I

Scheme 1: Schematic representation of the planar (D_{2h}) and *trans*-bent (C_{2h}) configurations of compounds **1-4**.

Further, we have estimated the contributions of the $\psi_{HOMO}(b_{3u})$ and $\psi_{LUMO}(b_{1u})$ molecular orbitals of compounds **1-4** in their corresponding vibronic coupling constants (F) and primary force constant (K_0) by means of canonical molecular orbital (CMO) approach.[47]

Computational details

CCSD(T)/Def2-TZVPP, MP2/Def2-TZVPP LC-BLYP/Def2-TZVPP, LC-ωPBE/Def2-TZVPP and B3LYP/Def2-TZVPP levels of theory were used to optimized the planar (D_{2h} symmetry) and *trans*-bent (C_{2h} symmetry) geometries of compounds **1-4** with the GAMESS US package of programs.[48,49] The nature of the stationary points of the ground and transition states for compounds **1-4** has been determined by means of the

number of imaginary frequencies.[50,51] The electronic configurations of the planar (D_{2h}) and *trans*-bent (C_{2h}) structures of compounds **1-4** were studied by means of time dependent density functional theory (TD-DFT), which is one of the most popular tools in the study of excited states of molecular systems.

The NBO 5.G program was performed at the B3LYP/Def2-TZVPP level to estimate quantitatively the magnitude of the plausible donor-acceptor hyperconjugative interactions for the planar (D_{2h}) and *trans*-bent (C_{2h}) structures of compounds **1-4**.[47]

The stabilization energies, off-diagonal elements, bonding and antibonding orbital energies and occupancies associated with $\pi_{M\text{-}M}(b_u)\rightarrow\sigma^*_{M\text{-}M}(b_u)$ electron delocalizations, natural bond orders (*nbo*) and natural atomic charges in the *trans*-bent structures of compounds **1-4** were analyzed by means of the NBO interpretations. The stabilization energies associated with donor→acceptor electron delocalizations are directly proportional to S^2 and also inversely proportional to $^1/_{\Delta E_{ij}}$ where S_{ij} is the orbital overlap integral and ΔE is the energy difference between the donor and acceptor orbitals.[52,53] There is a direct relationship between F_{ij} off-diagonal elements and the orbital overlap integral (S_{ij}).

In addition, the stabilization energy (E_2) associated with donor (i)→acceptor (j) electron delocalization is explicitly estimated by the following equation:

$$E_2 = q_i \frac{F_{ij}^2}{E_j - E_i} \qquad \text{(eq. 4)}$$

where q_i is the ith donor orbital occupancy, E_i, E_j are corresponded to the donor and acceptor orbitals, respectively.

Results and Discussion

1-*Planar and trans-bent interconversions*

CCSD(T)/Def2-TZVPP, LC-BLYP/Def2-TZVPP, LC-ωPBE/Def2-TZVPP, MP2/Def2-TZVPP and B3LYP/Def2-TZVPP corrected electronic energy (E_0=E_{el}+*ZPE*) differences between the planar (D_{2h}) and *trans*-bent (C_{2h}) geometries of compounds **1-4** are given in Tables 1 and SI-1. All methods used in this work showed the calculated barrier height for the $C_{2h}\rightarrow C_{2h}{}'$ interconversion processes *via* their corresponding planar (D_{2h}) forms [*i.e.* $C_{2h}\rightarrow(D_{2h})^{\neq}\rightarrow C_{2h}{}'$] are decreased from compound **1** to compound **4** (Figure 1).

It is worth noting that the presence of two or more electronic states (that are sufficiently and strongly interacting under nuclear displacement in the direction of instability) is the necessary and sufficient condition for instability of the high-symmetry configuration of any polyatomic system.[29-33] The normal modes of the planar (D_{2h}) forms of compounds **1-4** that lead them to the *trans*-bent (C_{2h}) forms are of b_{2g} symmetry. The imaginary wave numbers (corresponding to the imaginary vibrational frequencies) of the planar (D_{2h}) forms of compounds **1-4** are 351.79*i*, 244.94*i*, 225.51*i* and 205.12*i* cm^{-1}, respectively, as calculated at the B3LYP/Def2-TZVPP level of theory. There are significant correlations between the magnitudes of the imaginary wave numbers and barrier height for the $C_{2h} \rightarrow C_{2h}'$ interconversion processes *via* their corresponding planar (D_{2h}) forms [*i.e.* $C_{2h} \rightarrow (D_{2h})^{\neq} \rightarrow C_{2h}'$]. The force constants of the b_{2g} distortions of the planar (D_{2h}) configurations of compounds **1-4** are 1.8855, 1.0065, 0.8594 and 0.7059 mdyne $Å^{-1}$, respectively. Accordingly, the force constants of the corresponding b_{2g} distortions of D_{2h} configurations decrease from compound **1** to compound **4**. Based on this fact, one may expect that the *global hardness* (η) of the planar configurations should be decreased from compound **1** to compound **4**. The results of this work confirmed this expectation.

The distortions of high-symmetry (D_{2h}) configurations of compounds **1-4** are due to the pseudo Jahn-Teller effect (*PJTE*) [27-29]. The main contributions to the distortions of high-symmetry (D_{2h}) configurations to their corresponding *trans*-bent (C_{2h}) forms of compounds **1-4** are mainly due to the *PJTE* by mixing the ground A_g and excited B_{2g} states associated with mixing of $\psi_{HOMO}(b_{3u})$ and $\psi_{LUMO}(b_{1u})$ orbitals in compounds **1-4** resulting in a *PJT* $(A_g + B_{2g}) \otimes b_{2g}$ problem (see Figure 2).

The energies of the ground and excited states and their change along the distortion coordinate [Q_{b2g}] are shown in Figure 2. As it is shown from Figure 2, the curvatures of the lower curves (belongs to the ground state electronic configurations) of the *adiabatic potential energy surface* (*APES*) become negative but in the second upper sheet of compound **1** and also in the first upper sheets of compounds **2-4** (belongs to the excited electronic configurations which interact with the lower curves with respect to the Q_{b2g} displacements) the curvatures become positive.

The energy gaps between the reference states (Δ) in the planar (D_{2h}) configurations decrease from compound **1** to compound **4** (i.e. 2.67, 2.49, 2.08 and 1.64 eV for

compounds **1-4**, respectively) (Figure 2). One may expect that the *PJT* stabilization energy may increase by the decrease of the energy gaps between reference states (Δ), but there is different story for compounds **1-4**. Importantly, with the decrease of Δ values in the planar (D_{2h}) configurations from compound **1** to compound **4**, the corresponding *PJT* stabilization energies for $D_{2h} \rightarrow C_{2h}$ distortions decrease (Figures 1, 2).

The contributions of excited electronic states that should be involved in the structural changes are strongly diminished by the symmetry and the energy gaps between the interacting ground and excited states. It should be noted that only one, two or more excited states effectively take part in the softening of the high-symmetry configuration of the ground state. At least two electronic states of the reference configuration should be involved in rationalization of structural changes of any polyatomic system.[29-31]

We have examined several higher-lying excited states. It has to be noted that the higher-lying excited states have no contribution in the *PJT* interactions of compounds **1-4** (see Figure 2). By considering the curvatures K [i.e. $K=K_0-(F^2/\Delta)$] in the planar configurations (D_{2h}) of compounds **1-4** (see their imaginary vibrational frequencies which increase from compound **1** to compound **4**), we find that by the decrease of the energy gaps between reference states, Δ, the vibronic coupling constant (F) decrease from compound **1** to compound **4**. Interestingly, the decrease of the vibronic coupling constant, F, from compound **1** to compound **4** can be estimated from the canonical molecular orbital (CMO) analysis which gives full quantitative detail of the linear combinations of natural bond orbitals.

Since the main contributions to the distortions of high-symmetry (D_{2h}) configurations to their corresponding *trans*-bent (C_{2h}) forms of compounds **1-4** are mainly due to the *PJTE* by mixing the ground A_g and excited B_{2g} states, this mixing depends on the electronic wavefunctions of the orbitals which involve in the *PJTE* formalism. TD-DFT results indicate that in compounds **1-4** the *PJT* (A_g + B_{2g}) ⊗ b_{2g} problems are associated with mixing of $\psi_{HOMO}(b_{3u})$ and $\psi_{LUMO}(b_{1u})$ molecular orbitals. The magnitude of this mixing is correlated to the vibronic coupling constant, F, values.

We estimated the contributions of the corresponding molecular orbitals by means of canonical molecular orbital (CMO) method. In this approach, each molecular orbital ψ_i can be expressed in terms of the complete orthonormal set of natural bond orbitals.

In compounds **1-4**, the corresponding orbitals ψ_1 and ψ_2 are $\psi_{HOMO}(b_{3u})$ and $\psi_{LUMO}(b_{1u})$, respectively.

$$F = \left\langle \psi_{\mathrm{HOMO}}(B_{3u}) \middle| (\tfrac{\partial H}{\partial Q})_0 \middle| \psi_{\mathrm{LUMO}}(B_{1u}) \right\rangle \quad \text{(eq. 5)}$$

Based on the CMO results, full quantitative details of the linear combinations of natural bond orbitals in terms of the complete orthonormal set of NBOs in compounds **1-4** are given by the equations as follow:

Compound **1**:

$$\psi_{HOMO}(b_{3u}) = 0.948(\pi_{\mathrm{Si-Si}}) \quad \text{(eq. 6)}$$

$$\psi_{LUMO}(b_{1u}) = 0.407(\sigma^*_{\mathrm{Si-Si}}) - 3[0.403(\sigma^*_{\mathrm{Si-F}})] + 0.403(\sigma^*_{\mathrm{Si-F}}) \quad \text{(eq. 7)}$$

Compound **2**:

$$\psi_{HOMO}(b_{3u}) = 0.889(\pi_{\mathrm{Si-Si}}) - 4[0.225(\mathrm{LP\ Cl})] \quad \text{(eq. 8)}$$

$$\psi_{LUMO}(b_{1u}) = 0.385(\sigma^*_{\mathrm{Si-Si}}) - 3[0.427(\sigma^*_{\mathrm{Si-Cl}})] + 0.427(\sigma^*_{\mathrm{Si-Cl}}) \quad \text{(eq. 9)}$$

Compound **3**:

$$\psi_{HOMO}(b_{3u}) = 0.863(\pi_{\mathrm{Si-Si}}) - 4[0.249(\mathrm{LP\ Br})] \quad \text{(eq. 10)}$$

$$\psi_{LUMO}(b_{1u}) = 0.345(\sigma^*_{\mathrm{Si-Si}}) - 3[0.439(\sigma^*_{\mathrm{Si-Br}})] + 0.439(\sigma^*_{\mathrm{Si-Br}}) \quad \text{(eq. 11)}$$

Compound **4**:

$$\psi_{HOMO}(b_{3u}) = 0.819(\pi_{\mathrm{Si-Si}}) - 4[0.283(\mathrm{LP\ I})] \quad \text{(eq. 12)}$$

$$\psi_{LUMO}(b_{1u}) = 0.304(\sigma^*_{Si-Si}) - 3[0.446(\sigma^*_{\mathrm{Si-I}})] + 0.446(\sigma^*_{\mathrm{Si-I}}) \quad \text{(eq. 13)}$$

The results obtained showed that the coefficients of the $\pi_{\mathrm{Si\text{-}Si}}$ bonding orbitals in the $\psi_{HOMO}(b_{3u})$ molecular orbitals decrease from compound **1** to compound **4** (see eqs. 8-15). Similar trend observed for the coefficients of the $\sigma^*_{\mathrm{Si\text{-}Si}}$ anti-bonding orbitals in the $\psi_{LUMO}(b_{1u})$ molecular orbitals. Interestingly, this fact explicitly can be found from Fig. 3

ongoing from compound **1** to compound **4**. Accordingly, by considering the equations 1-13, the *PJT* vibronic coupling constants and primary force constant (the force constant without the *PJTE*, K_0) decrease from compound **1** to compound **4**. This fact clearly justifies the decrease of the E_{PJT} ongoing from compound **1** to compound **4**.

2-*Structural parameters*

The structural parameters of the planar (D_{2h}) and *trans*-bent (C_{2h}) configurations of compounds **1-4** as calculated at the CCSD(T)/Def2-TZVPP, LC-ωPBE/Def2-TZVPP, B3LYP/Def2-TZVPP and MP2/Def2-TZVPP levels of theory are given in Tables 2 and SI-2. All methods used showed that the flap angles between the X_2Si planes and the Si=Si bonds in the distorted (*trans*-bent, C_{2h}) configurations decrease from compound **1** to compound **4** (Scheme 2). The results obtained at all levels of theory used in this work were compared with the published X-ray diffraction (XRD) data for the Si_2Cl_4 species which was stabilized as (Cy-cAAC·)$_2Si_2Cl_4$ complex utilizing two cAAC (cyclic alkyl(amino)carbine) chelating groups (Table 2).[27] The longer Si-Si bond length in (Cy-cAAC·)$_2Si_2Cl_4$ compared to compound **2** is attributed to the presence of the Cy-cAAC· chelating groups, causing more trans-bending in the Si_2Cl_4 species (Table 2).

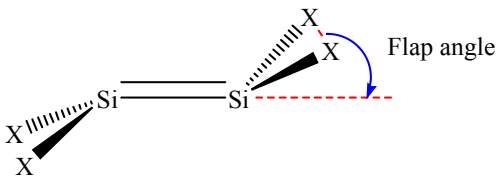

Scheme 2: Schematic representation of the flap angles in the *trans*-bent (C_{2h}) structures of compounds **1-4**.

All methods used showed that the r_{Si-Si} bond lengths in the *trans*-bent (C_{2h}) configurations are decreased ongoing from compound **1** to compound **4** which results from the decrease of their corresponding flap-angles. It is worth noting that the r_{Si-Si} bond lengths in the *trans*-bent (C_{2h}) configurations of compounds **1-4** are longer than those of their corresponding planar structures (D_{2h}). This fact is attributed to the greater bond orders of the planar configurations of compounds **1-4** (due to the maximum p-orbitals overlap of Si atoms) compared to their corresponding *trans*-bent (C_{2h}) structures. The small bond

order values of the *trans*-bent (C_{2h}) configurations of compounds **1-4** can be explained by the deviations of the p-orbitals of Si atoms (which are responsible for the formation of the π bonds between Si atoms) from their values in the planar configurations (i.e. 90º).

The results of all three levels of theory showed that the calculated bond length differences between the Si=Si bonds in the planar (D_{2h}) and *trans*-bent (C_{2h}) configurations (i.e. $\Delta[r_{Si\text{-}Si}(C_{2h})\text{-}r_{Si\text{-}Si}(D_{2h})]$) decrease from compound **1** to compound **4** (see Table 2). It is interesting to note that there is a linear correlation between E_{PJT} versus $\Delta[r_{Si\text{-}Si}(C_{2h})\text{-}r_{Si\text{-}Si}(D_{2h})]$ in compounds **1-4** (Figure 3). The decrease of $\Delta[r_{Si\text{-}Si}(C_{2h})\text{-}r_{Si\text{-}Si}(D_{2h})]$ parameter is in accordance with the decrease of the E_{PJT} ongoing from compound **1** to compound **4**. Therefore, $\Delta[r_{Si\text{-}Si}(C_{2h})\text{-}r_{Si\text{-}Si}(D_{2h})]$ parameter can be proposed as a criterion for the evaluation of the E_{PJT} in compounds **1-4**.

3-*Global hardness and electronegativity*

The energies of the highest unoccupied and lowest occupied molecular orbitals (LUMO and HOMO) of the planar (D_{2h}) and *trans*-bent (C_{2h}) configurations of compounds **1-4**, as calculated at the B3LYP/Def2-TZVPP level of theory, are given in Table 3. The energies of the HOMOs (ε_{HOMO}) increase from the planar (D_{2h}) configurations of compound **1** to compound **4** but the energies of the LUMOs decrease. Also, the energies of the HOMOs (ε_{HOMO}) in the *trans*-bent (C_{2h}) configurations increase from compound **1** to compound **4**. The energies of the LUMOs (ε_{LUMO}) decrease from the *trans*-bent (C_{2h}) configurations of compound **1** to compound **3** but increases from compound **3** to compound **4**. Effectively, the energy gaps between the HOMO and LUMO orbitals (i.e. $E_{LUMO}\text{-}E_{HOMO}$) decrease from the planar (D_{2h}) and *trans*-bent (C_{2h}) configurations of compound **1** to compound **4**.

Hardness can be interpreted in terms of the separations of the frontier molecular orbitals (i.e. the HOMO-LUMO gap).[54-57] The relationship between the global *hardness* (η),[54-56] global *electronegativity* (χ),[57] ionization potential and electron affinity of a molecule is defined as the following expression:

$\eta = 0.5\ (I - A)$ (eq. 14)

$\chi = 0.5\ (I + A)$ (eq. 15)

where I and A are ionization potential and electron affinity of the molecules, respectively.[54-57] By considering the validity of Koopmans' theorem, the hardness (η) and electronegativity (χ) can be written as:

$\eta = 0.5\ (\varepsilon_{LUMO}-\varepsilon_{HOMO})$ (eq. 16)

$\chi = -0.5\ (\varepsilon_{LUMO}+\varepsilon_{HOMO})$ (eq. 17)

As can be seen from Table 4, global hardness values of the *trans*-bent (C_{2h}) configurations decrease from compound **1** to compound **4**. Figure 4 shows the a linear correlation from the plot of the E_{PJT} versus global hardness of the *trans*-bent (C_{2h}) structures [$\eta(C_{2h})$] in compounds **1-4**.

The results obtained showed that the *trans*-bent (C_{2h}) configuration of compounds **1** and **4** are harder than their corresponding planar (D_{2h}) configuration but an opposite trend observed for compounds **2** and **3**. Therefore, the hardest configurations of compounds **2** and **3** are not the most stable forms of these compounds. Accordingly, the configurational properties of compounds **1-4** do not obey the *maximum hardness principle*.[55]

Using the hardness values obtained, a "Δ" parameter can be found as $\Delta[\eta(C_{2h})-\eta(D_{2h})]$. The calculated $\Delta[\eta(C_{2h})-\eta(D_{2h})]$ parameter decreases from compound **1** to compound **2** but increases from compound **2** to compound **4**. Accordingly, the variations of $\Delta[\eta(C_{2h})-\eta(D_{2h})]$ parameters do not explain the variations of the barrier heights for the $C_{2h}\rightarrow C_{2h}'$ interconversion processes *via* their corresponding planar (D_{2h}) forms [*i.e.* $C_{2h}\rightarrow(D_{2h})^{\neq}\rightarrow C_{2h}'$] from compound **1** to compound **4**.

The results of this work showed that the global *electronegativity* (χ)[50] values of the *trans*-bent (C_{2h}) configurations of compounds **1-4** are greater than those of their corresponding planar (D_{2h}) configurations. It has to be noted that the global *electronegativity*, χ, determines the Lewis acid or base character of a molecule. Molecules with a large χ values are characterized as the strong Lewis acids and small χ values are found for the strong Lewis bases. Based on the global *electronegativity* (χ) values obtained for the *trans*-bent (C_{2h}) structures, compound **1** is a stronger Lewis acid compared to compound **2**. In this context, there is no significant difference between the Lewis acid characters of compounds **2** and **3** but compound **4** is weaker than them.

Using the global *electronegativity* values obtained for the *trans*-bent (C_{2h}) and planar (D_{2h}) configurations of compounds **1-4**, "Δ" parameters were found as Δ[$\chi(C_{2h})$ - $\chi(D_{2h})$]. Interestingly, the calculated Δ[$\chi(C_{2h})$-$\chi(D_{2h})$] parameters decrease from compound **1** to compound **4**. The variations of Δ[$\chi(C_{2h})$-$\chi(D_{2h})$] parameters from compound **1** to compound **4** are in the trend observed for the decrease of their corresponding *PJT* stabilization energies for the $D_{2h}\rightarrow C_{2h}$ conversion processes. Accordingly, the variations of Δ[$\chi(C_{2h})$-$\chi(D_{2h})$] parameters succeed in accounting for the decrease of the E_{PJT} from compound **1** to compound **4** (see Tables 1, 3).

Due to the inherent self-interaction errors, the B3LYP kernel often underestimates the energies of the HOMOs and LUMOs of some molecular systems whereas the range-separated density functional theories such as long range-corrected (LRC) hybrids (e.g. LC-ωPBE/Def2-TZVPP and LC-BLYP/Def2-TZVPP) are expected to give more accurate results.[58-60] However, the quantities of interest here (i.e. Δ[$\chi(C_{2h})$-$\chi(D_{2h})$] parameter) are the relative values for different forms of the same molecule. We expect that the errors in such parameters will be very small and that even the corresponding errors between the different closely related compounds will be minimal. The smooth variation among the calculated values confirms this expectation.

In order to compare the results of the B3LYP/Def2-TZVPP method with the long range-corrected hybrids, we performed the LC-ωPBE/Def2-TZVPP and LC-BLYP/Def2-TZVPP levels to calculate the energies of the HOMOs and LUMOs of the *trans*-bent (C_{2h}) and planar (D_{2h}) configurations of compounds **1-4** (Tables SI-3 and SI-4). Although the B3LYP/Def2-TZVPP level overestimates the energies of the HOMOs and LUMOs of the *trans*-bent (C_{2h}) and planar (D_{2h}) configurations of compounds **1-4** compared to those obtained at the LC-ωPBE/Def2-TZVPP and LC-BLYP/Def2-TZVPP levels, the trend observed for the variations of Δ[$\eta(C_{2h})\eta$-(D_{2h})] and Δ[$\chi(C_{2h})$-$\chi(D_{2h})$] parameters form compound **1** to compound **4** at these three levels are the same (Tables 3, SI-3, SI-4).

4-*Stabilization energies associated with the electron delocalizations*

Figures 1 and 2 shows the *PJT* stabilization energies decrease from compound **1** to compound **4**. The canonical molecular orbital analysis revealed that the E_{PJT} is due to the mixing of the ground A_g and excited B_{2g} electronic states associated with mixing of HOMO

(b_{3u}, $\pi_{Si\text{-}Si}$) and LUMO(b_{1u}, $\sigma^*_{Si\text{-}Si}$) orbitals. It should be noted that *PJT* distortions in the planar configurations of compounds **1-4** ($D_{2h}\rightarrow C_{2h}$) along b_{2g} displacement reduces the symmetry of mixing b_{3u} and b_{1u} orbitals to b_u. NBO results showed that with mixing of the donor $\pi_{Si\text{-}Si}(b_u)$ bonding and acceptor $\sigma^*_{Si\text{-}Si}(b_u)$ antibonding orbitals, their corresponding electron delocalizations decrease from the *trans*-bent (C_{2h}) configurations of compound **1** to compound **4** (Table 4). A linear correlation is also found from the plot of the E_{PJT} versus the stabilization energies (E_2) associated with $\pi_{Si\text{-}Si}\rightarrow\sigma^*_{Si\text{-}Si}$ electron delocalizations (Figure 5). It is worth noting that the decrease of the *trans*-bending from compound **1** to compound **4** can be interpreted by the decrease of the $\pi_{Si\text{-}Si}\rightarrow\sigma^*_{Si\text{-}Si}$ electron delocalization (Scheme 3).

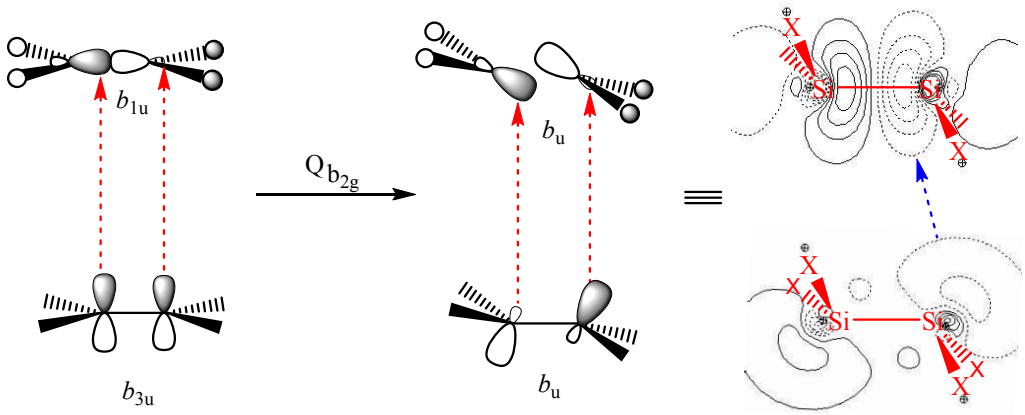

X = F (**1**), Cl (**2**), Br (**3**), I (**4**)

Scheme 3. Pseudo Jahn-Teller distortion in the planar configurations of compounds **1-4** ($D_{2h}\rightarrow C_{2h}$) along b_{2g} displacement reduces the symmetry of mixing b_{3u} and b_{1u} orbitals to b_u.

5-Orbital occupancies

The NBO interpretation was used to investigate the variations of the occupancies of the donor and acceptor orbitals which are responsible for the distortion of the planar (D_{2h}) configurations of compounds **1-4** [i.e $\pi_{M\text{-}M}(b_u)\rightarrow \sigma^*_{M\text{-}M}(b_u)$ electron delocalization]. The

NBO analysis showed that the $\pi_{M\text{-}M}(b_u)$ bonding orbital occupancies of the *trans* bent (C_{2h}) configurations increase from compound **1** to compound **4** while the occupancies of the $\sigma^*_{M\text{-}M}(b_u)$ anti-bonding orbital decrease (Table 4). The trend observed for the electron depletions from the $\pi_{M\text{-}M}(b_u)$ bonding orbitals and electron accumulations in the $\sigma^*_{M\text{-}M}(b_u)$ anti-bonding orbitals can be justified by the decrease of the $\pi_{M\text{-}M}(b_u) \rightarrow \sigma^*_{M\text{-}M}(b_u)$ electron delocalizations from the *trans* bent (C_{2h}) configurations of compound **1** to compound **4**.

6-*Orbital energies and off-diagonal elements*

The stabilization energy associated with the electron delocalization should increase as the acceptor orbital energy decreases and the donor orbital energy increases. The energy differences between donor [$\pi_{M\text{-}M}(b_u)$] and acceptor [$\sigma^*_{M\text{-}M}(b_u)$] orbitals ([i.e. $\Delta[E\ \sigma^*_{M\text{-}M}(b_u) - E\ \pi_{M\text{-}M}(b_u)]$]) for the *trans*-bent configurations of compounds **1-4** are 0.27088, 0.32092, 0.32206 and 0.33869 a.u., respectively. The energy of the acceptor $\sigma^*_{M\text{-}M}(b_u)$ anti-bonding orbital increases from the *trans*-bent structure of compound **1** to compound **2** but decreases from compound **2** to compound **3** and increases from compound **3** to compound **4**. Accordingly, the variations of the energies of acceptor $\sigma^*_{M\text{-}M}(b_u)$ anti-bonding orbitals do not explain the decrease of the energy gaps between the donor $\pi_{M\text{-}M}(b_u)$ bonding orbitals and the acceptor $\sigma^*_{M\text{-}M}(b_u)$ anti-bonding orbitals. The strong donor bonding orbital (i.e. E $\pi_{M\text{-}M}(b_u)$ = -0.22989 a.u.) of compound **1** [compared to those in compounds **2**-**4**, -.27617, -0.28673 and -0.29189 a.u. respectively] gives rise to strong electron delocalization (Table 4). The decrease of the energies of the donor $\pi_{M\text{-}M}(b_u)$ bonding orbitals from compound **1** to compound **4** controls the variations of their corresponding differences between donor [$\pi_{M\text{-}M}(b_u)$] and acceptor [$\sigma^*_{M\text{-}M}(b_u)$] orbitals [i.e. $\Delta(\varepsilon[\sigma^*_{M\text{-}M}(b_u)]\text{-}\varepsilon[\pi_{M\text{-}M}(b_u)])$]. Accordingly, the increase of $\Delta(\varepsilon[\sigma^*_{M\text{-}M}(b_u)]\text{-}\varepsilon[\pi_{M\text{-}M}(b_u)])$ parameters from compound **1** to compound **4** has a determinant impact on the variations of their corresponding $\pi_{M\text{-}M}(b_u) \rightarrow \sigma^*_{M\text{-}M}(b_u)$ electron delocalizations.

It should be noted that the off-diagonal elements (F_{ij}) for the $\pi_{M\text{-}M}(b_u) \rightarrow \sigma^*_{M\text{-}M}(b_u)$ electron delocalizations decrease from the *trans*-bent configurations of compound **1** to compound **4**. Therefore, there is no conflict between the off-diagonal elements (F_{ij}) and $\Delta(\varepsilon[\sigma^*_{M\text{-}M}(b_u)]\text{-}\varepsilon[\pi_{M\text{-}M}(b_u)])$ parameters for $\pi_{M\text{-}M}(b_u) \rightarrow \sigma^*_{M\text{-}M}(b_u)$ electron delocalization in the *trans*-bent configurations of compounds **1-4**.

7-*Bond orders*

The bond lengths and bond orders of Si-Si bonds of the *trans*-bent configurations of compounds **1-4** can be affected from the variations of $\pi_{si\text{-}si} \rightarrow \sigma^*_{si\text{-}si}$ electron delocalizations. The NBO-B3LYP/Def2-TZVPP calculated natural bond orders [*nbo*] of the Si-Si bonds in the *trans*-bent (C_{2h}) configurations of compound **1-4** are 1.281, 1.470, 1.487 and 1.531, respectively. Importantly, the calculated natural bond order differences between the Si and X atoms in the *trans*-bent (C_{2h}) configurations (i.e. Δ[*nbo*(Si-Si)-*nbo*(Si-X)]) increase from compound **1** to compound **4**. This fact demonstrates that the $\pi_{si\text{-}si}$ bond strength increases from the *trans*-bent (C_{2h}) configurations of compound **1** to compound **4**. Accordingly, the increase of the Si-Si bond strength from compound **1** to compound **4** can results from the decrease of their corresponding $\pi_{si\text{-}si}$ (b_u)→ $\sigma^*_{si\text{-}si}$ (b_u) electron delocalization (Table 4).

8-*Natural charges*

The calculated natural atomic charges (*NAC*, nuclear charge minus summed natural populations of natural atomic orbitals on the atom) of the Si and X (F, Cl, Br, I) atoms in the *trans*-bent structures of compounds **1-4** are given in Table 3. The calculated natural atomic charge differences between the Si and X atoms in the *trans*-bent structures (C_{2h}) (i.e. Δ[*NAC* (Si)-*NAC* (X)]) decrease from compound **1** to compound **4** (Table 4). The decrease of Δ[*NAC* (Si)-*NAC* (X)] parameter can be justified by the decrease of the X atom electronegativity ongoing from Fluorine to Iodine atoms. There is a linear correlation between for the plot of the E_{PJT} and Δ[*NAC* (Si)-*NAC* (X)] parameters (Figure 6). Accordingly, Δ[*NAC* (Si)-*NAC* (X)] parameter can also be considered as another criterion for the estimation of the *PJT* distortion in compounds **1-4**.

Conclusion

The CCSD(T), B3LYP, LC-BLYP, LC-ωPBE and MP2 calculations reported above and the NBO interpretations provide a reasonable picture for the correlations between the *PJTE* parameters (*i.e. F*, Δ and K_0), the structural and configurational properties of compounds **1-4**. The results obtained showed that the *trans-bent* (C_{2h}) structures of compounds **1-4** are more stable than their corresponding planar (D_{2h}) configurations and the energy differences between the D_{2h} and C_{2h} configurations decrease

from compound **1** to compound **4**. The distortions in the planar (D_{2h}) configurations of compounds **1-4** are due to the *PJTE*, resulting from mixing of the ground A_g and excited B_{2g} states [i.e. *PJT* ($A_g + B_{2g}$) $\otimes$ b_{2g} problem]. Surprisingly, contrary to usual expectations, with the decrease of the energy gaps between reference states (Δ) in the undistorted (D_{2h}) configurations from compound **1** to compound **4**, their corresponding *PJT* stabilization energies decrease. We analyzed quantitatively the details of the linear combinations of natural bond orbitals and the results obtained showed that the F and K_0 values decrease with decrease of the coefficients of the $\pi_{si\text{-}si}$ bonding and $\sigma^*_{si\text{-}si}$ anti-bonding orbitals in the $\psi_{HOMO}(b_{3u})$ and $\psi_{LUMO}(b_{1u})$ molecular orbitals from compound **1** to compound **4**. This fact justifies the decrease of the *PJT* stabilization energies ongoing from compound **1** to compound **4**. Effectively, the decrease of the stabilization energies associated with the mixing of the donor $\pi_{si\text{-}si}(b_u)$ bonding and acceptor $\sigma^*_{si\text{-}si}(b_u)$ antibonding orbitals in the distorted (C_{2h}) configurations of compounds **1-4** correlates well with the decrease their corresponding *PJT* stabilization energies along the b_{2g} bending. It should be noted that the variations of the global hardness (η) differences between the *trans*-bent (C_{2h}) and planar (D_{2h}) configurations of compounds **1-4** do not correlate with the decrease of their corresponding *PJT* stabilization energies. Interestingly, the variations of the global electronegativity (χ) differences between the *trans*-bent (C_{2h}) and planar (D_{2h}) configurations succeed in accounting for the decrease of the *PJT* stabilization energies for the $D_{2h} \rightarrow C_{2h}$ conversion processes from compound **1** to compound **4**.

Acknowledgement: Davood Nori-Shargh wishes to thank Professor Dr. Issac B. Bersuker for very useful and instructive discussions.

References

1. K. Krogh-Jespersen, *J. Phys. Chem.* 1982, **86**, 1492.
2. G. Olbrich, *Chem. Phys. Lett.* 1986, **130**, 115.
3. K. Somasundran, R. D. Amos, N. C. Handy, *Theor. Chim. Acta.* 1986, **70**, 393.
4. H. Teramae, *J. Am. Chem. Soc.* 1987, **109**, 4140.
5. G. Trinquier, J. P. Malrieu, P. Rivière, *J. Am. Chem. Soc.* 1982, **104**, 4529.
6. T. Fjeldberg, M. F. Lappert, B. E. R. Schilling, R. Seip, A. J. Thorne, *J. Chem. Soc., Chem. Commun.* 1982, **24**, 1407.
7. S. Nagase, T. Kudo, *J. Mol. Struct. (THEOCHEM)* 1983, **103**, 35.
8. D. E. Goldberg, P. B. Hitchcock, M. F. Lappert, K. M. Thomas, A. J. Thorne, T. Fjeldberg, A. Haaland, B. E. R. Schilling, *J. Chem. Soc., Dalton Trans.* 1986, 2387.
9. G. Trinquier, J. P. Malrieu, *J. Phys. Chem.* 1990, **94**, 6184.
10. G. Trinquier, J. P. Malrieu, *J. Am. Chem. Soc.* 1987, **109**, 5303.
11. J. P. Malrieu, G. Trinquier, *J. Am. Chem. Soc*. 1989, **111**, 5916.
12. H. J. Kohlerm, H. Lischka, *J. Am. Chem. Soc.* 1982, **104**, 5884.
13. M. W. Schmidt, P. N. Truong, M. S. Gordon, *J. Am. Chem. Soc.* 1987, **109**, 5217.
14. G. Trinquier, *J. Am. Chem. Soc.* 1990, **112**, 2130.
15. G. Trinquier, J. –C. Barthelat, *J. Am. Chem. Soc.* 1990, **112**, 9121.
16. H. Jacobsen, T. Zeigler, *J. Am. Chem. Soc.* 1994, **116**, 3667.
17. B. R. Streit, D. K. Geiger, *J. Chem. Edu.* **2005**, 82, 111-116.
18. D. Nori-Shargh, S. N. Mousavi, J. E. Boggs, *J. Phys. Chem. A* 2013 **117**, 1621.
19. M. T. Swihart, M. T. Carr, *J. Phys. Chem. A* 1998, **102**, 785.
20. A. H. Cowley, *Polyhedron.* 1984, **3**, 389.
21. A. H. Cowley, *Acc. Chem. Res.* 1984, **17**, 386.
22. G. Raabe, J. Michl, *Chem. Rev.* 1985, **85**, 419.
23. A. H. Cowley, N. C. Norman, *Prog. Inorg. Chem*. 1986, **34**, 1.
24. R. West, *Angew. Chem. Int. Ed. Engl.* 1987, **26**, 1201.
25. C. Liang, L. C. Allen, *J. Am. Chem. Soc.* 1990, **112**, 1039.
26. A. V. Lalov, S. E.Boganov, V. I. Faustov, M. P.Egorov, O. M. Nefedov, *Russ. Chem. Bull*. 2003, **52**, 526.
27. M. Karni, Y. Apeloig, *J. Am. Chem. Soc.* 1990, **112**, 8589.

28. K. C. Mondal, B. Dittrich, B. Maity, D. Koley, H. W. Roesky, *J. Am. Chem. Soc*. 2014, **136**, 9568.
29. I. B. Bersuker, *Chem. Rev.* 2001, **101**, 1067.
30. I. B. Bersuker, *The Jahn-Teller Effect*, Cambridge University Press: New York, 2006.
31. I.B. Bersuker, *Chem. Rev*. 2013, **113**, 1351.
32. I. B. Bersuker, *Phys. Rev. Lett*. 2012, **108**, 137202.
33. H. Köppl, D. R. Yarkoni, Barentzen, L. (Eds.), *The Jahn-Teller Effect: Fundamentals and Implications for Physics and Chemistry*, Springer-Verlag Berlin Heidelberg, 2009.
34. H. Kayi, P. Garcia-Fernandez, I. B. Bersuker, J. E. Boggs, *J. Phys. Chem. A* 2013, **117**, 8671.
35. H. Kayi, I. B. Bersuker, J. E. Boggs, *J. Mol. Struct*. 2012, **1023**, 108.
36. Y. Liu, I. B. Bersuker, W. Zou, J. E. Boggs, *J. Chem. Theory Comput*. 2009, **5**, 2679.
37. W. Zou, M. Filatov, D. Cremer, *Int. J. Quant. Chem*. 2012, **112**, 3277.
38. P. Garcia-Fernandez, Y. Liu, I. B. Bersuker, J. E. Boggs, *Phys. Chem. Chem. Phys.* 2011, **13**, 3502.
39. E. Runge, E. K. U. Gross, *Phys. Rev. Lett*. 1984, **52**, 997.
40. A. D. Becke, *J. Chem. Phys*. 1993, **98**, 5648.
41. F. Weigend, *Phys. Chem. Chem. Phys.* 2006, **8**, 1057.
42. M. Urban, J. Noga, S. J. Cole, R. J. Bartlett, *J. Chem. Phys.* 1985, **83**, 4041.
43. C. Møller, M. S. Plesset, *Phys. Rev*. 1934, **46**, 618.
44. D. Cremer, in Encyclopedia of Computational Chemistry, edited by P. v. R. Schleyer, Wiley, New York, 1998.
45. Y. Tawada, T. Tsuneda, S. Yanagisawa, T. Yanai, K. Hirao, *J. Chem. Phys*. 2004, **120**, 8425.
46. O. A. Vydrov, G. E. Scuseria, *J. Chem. Phys*. 2006, **125**, 234109.
47. E. D. Glendening, J. K. Badenhoop, A. E. Reed, J. E. Carpenter, J. A. Bohmann, C. M. Morales, F. Weinhold, *Theoretical Chemistry Institute, University of Wisconsin*, Madison, WI, NBO Version 5.G, 2004.
48. M. W. Schmidt, K. K. Baldridge, J. A. Boatz, S. T. Elbert, M. S. Gordon, J. H. Jensen, S. Koseki, N. Matsunaga, K. A. Nguyen, S. J. Su, T. L. Windus, M. Dupuis, J. A. Montgomery, *J. Comput. Chem*. 1993, **14**, 1347.

49. M. S. Gordon, M. W. Schmidt, *Advances in electronic structure theory: GAMESS a decade later*, In: C. E. Dykstra, G. Frenking, K. S. Lim, G. E. Scusaria, *Theory and Applications of Computational Chemistry, the first 40 years*, Amsterdam, Elsevier, 2005.
50. J. W. McIver, Jr. *Acc. Chem. Res*. 1974, **7**, 72.
51. O. Ermer, *Tetrahedron*. 1975, **31**, 1849.
52. P. Dionne, M. St-Jacques, *J. Am. Chem. Soc.* 1987, **109**, 2616.
53. N. B. Epiotis, R. L. Yates, R. J. Larson, C. R. Kirmaier, F. Bernardi, *J. Am. Chem. Soc.* 1977, **99**, 8379.
54. R. G. Parr, R. G. Pearson, *J. Am. Chem. Soc*. 1983, **105**, 7512.
55. R. G. Pearson, W. E. Palke, *J. Phys. Chem*. 1992, **96,** 3283.
56. R. G. Pearson, *J. Chem. Educ*. 1987, **64**, 561.
57. R. G. Parr, R. A. Donnelly, M. Levy, W. E. Palke, *J. Chem. Phys*. 1978, **68**, 3801.
58. A. F. Izmaylov, G. E. Scuseria, *J. Chem. Phys*. 2008, **129**, 034101.
59. M. E. Foster, B. M. Wong, *J. Chem. Theory Comput*. 2012, **8**, 2682.
60. T. Körzdörfer, J. S. Sears, C. Sutton, J.-L. Brédas, *J. Chem. Phys*. 2011, **135**, 204107.

Table 1. CCSD(T)/Def2-TZVPP, LC-ωPBE/Def2-TZVPP, MP2/Def2-TZVPP and B3LYP/Def2-TZVPP calculated corrected electronic energies (E_o=E_{el}+*ZPE* for the planar (D_{2h}) and *trans*-bent (C_{2h}) geometries of compounds **1-4**.

Method	B3LYP/Def2-TZVPP			LC-ωPBE/Def2-TZVPP			MP2/Def2-TZVPP		CCSD(T)/Def2-TZVPP	
	ZPE[b]	E_0	ΔE_0^a	*ZPE*	E_0	ΔE_0^a			E_0	ΔE_0^a
compound										
1, C_{2h}	0.011062	-977.265983	0.00	0.011243	-978.325617	0.00	-977.220823	0.00	-978.789737	0.00
1, D_{2h}	0.012652	-977.213602	32.87	0.012978	-978.282672	26.95	-977.161802	37.04	-978.731386	36.62
2, C_{2h}	0.007288	-2417.159505	0.00	0.007967	-2419.291896	0.00	-2417.036433	0.00	-2420.099696	0.00
2, D_{2h}	0.008152	-2417.133494	16.32	0.008707	-2419.278261	8.56	-2417.013226	14.56	-2420.069176	19.15
3, C_{2h}	0.005644	-10869.073720	0.00	0.006360	-10874.132689	0.00	-10868.993490	0.00	-10875.913622	0.00
3, D_{2h}	0.006350	-10869.051480	13.96	0.006902	-10874.122226	6.56	-10868.973310	12.66	-10875.885970	17.35
4, C_{2h}	0.004864	-1767.133691	0.00	0.005588	-1769.887986	0.00	-1767.201373	0.00	-1770.373083	0.00
4, D_{2h}	0.005336	-1767.117361	10.25	0.005848	-1769.881968	3.78	-1767.185434	10.00	-1770.351212	13.72

[a] Relative to the most stable form (C_{2h}). [b] The calculated zero point energies (*ZPE*) at the B3LYP/Def2-TZVPP level were used to calculate the corrected electronic energies at the MP2/Def2-TZVPP and CCSD(T)/Def2-TZVPP levels.

Table 2. Calculated structural parameters of the planar (D_{2h} symmetry) and *trans*-bent (C_{2h}) geometries of compounds **1-4**.

Compound	**1**		**2**		**3**		**4**	
Geometry	D_{2h}	C_{2h}	D_{2h}	C_{2h}	D_{2h}	C_{2h}	D_{2h}	C_{2h}
Bond lengths (Å)								
$r_{si\text{-}si}$	(2.094)[a] (2.064)[b] (2.084)[c] (2.086)[d] (2.048)[e]	(2.548)[a] (2.641)[b] (2.638)[c] (2.582)[d]	(2.117)[a] (2.083)[b] (2.113)[c] (2.112)[d]	(2.349)[a] (2.311)[b] (2.426)[c] (2.334)[d] (2.343)[f] (2.454)[g] (2.446)[h]	(2.124)[a] (2.090)[b] (2.123)[c] (2.121)[d]	(2.310)[a] (2.273)[b] (2.404)[c] (2.309)[d]	(2.138)[a] (2.101)[b] (2.140)[c] (2.135)[d]	(2.284)[a] (2.220)[b] (2.365)[c] (2.280)[d]
$r_{si\text{-}x}$	(1.580)[a] (1.581)[b] (1.584)[c] (1.582)[d] (1.591)[e]	(1.596)[a] (1.598)[b] (1.604)[c] (1.598)[d]	(2.029)[a] (2.012)[b] (2.036)[c] (2.021)[d]	(2.059)[a] (2.038)[b] (2.076)[c] (2.051)[d] (2.056)[f]	(2.189)[a] (2.170)[b] (2.204)[c] (2.178)[d]	(2.223)[a] (2.197)[b] (2.249)[c] (2.212)[d]	(2.406)[a] (2.385)[b] (2.429)[c] (2.385)[d]	(2.439)[a] (2.409)[b] (2.477)[c] (2.422)[d]
$\Delta[r_{si\text{-}si}(C_{2h})- r_{si\text{-}si}(D_{2h})]$[a]	0.454		0.232		0.186		0.146	
$\Delta[r_{si\text{-}si}(C_{2h})- r_{si\text{-}si}(D_{2h})]$[b]	0.468		0.228		0.200		0.140	
$\Delta[r_{si\text{-}si}(C_{2h})- r_{si\text{-}si}(D_{2h})]$[c]	0.554		0.313		0.281		0.225	
$\Delta[r_{si\text{-}si}(C_{2h})- r_{si\text{-}si}(D_{2h})]$[d]	0.496		0.222		0.188		0.145	
Bond angles (°)								
$\theta_{x\text{-}si\text{-}si}$	(125.3)[a] (125.3)[b] (125.1)[c] (125.2)[d]	(107.3)[a] (106.6)[b] (106.7)[c] (107.4)[d]	(123.1)[a] (123.2)[b] (123.0)[c] (123.0)[d]	(111.0)[a] (112.1)[b] (110.2)[c] (111.0)[d] (111.0)[e]	(122.4)[a] (122.7)[b] (122.5)[c] (122.2)[d]	(111.2)[a] (112.8)[b] (110.4)[c] (111.1)[d]	(121.4)[a] (121.7)[b] (121.7)[c] (121.1)[d]	(111.8)[a] (114.2)[b] (111.1)[c] (111.1)[d]
$\theta_{x\text{-}si\text{-}x}$	(109.4)[a] (109.5)[b] (109.8)[c] (109.6)[d] (109.7)[e]	(102.4)[a] (102.3)[b] (102.8)[c] (103.2)[d]	(113.8)[a] (113.5)[b] (114.0)[c] (114.0)[d]	(107.4)[a] (106.8)[b] (106.1)[c] (107.3)[d]	(115.2)[a] (114.6)[b] (115.1)[c] (115.5)[d]	(108.6)[a] (108.2)[b] (107.3)[c] (108.8)[d]	(117.2)[a] (116.6)[b] (116.7)[c] (117.8)[d]	(110.2)[a] (110.9)[b] (109.0)[c] (111.0)[d]
Torsion angles (°)								
$\theta_{x\text{-}si\text{-}si\text{-}x}$	(0.0)[a] (0.0)[b] (0.0)[c] (0.0)[d]	(70.5)[a] (71.3)[b] (70.5)[c] (69.6)[d]	(0.0)[a] (0.0)[b] (0.0)[c] (0.0)[d]	(60.7)[a] (60.0)[b] (63.3)[c] (60.7)[d] (61.0)[f]	(0.0)[a] (0.0)[b] (0.0)[c] (0.0)[d]	(58.8)[a] (57.0)[b] (61.5)[c] (58.8)[d]	(0.0)[a] (0.0)[b] (0.0)[c] (0.0)[d]	(55.9)[a] (50.8)[b] (58.4)[c] (55.9)[d]
Flap Angles (°)								
	(0.0)[a] (0.0)[b] (0.0)[c] (0.0)[d]	(61.6)[a] (62.9)[b] (62.4)[c] (61.2)[d]	(0.0)[a] (0.0)[b] (0.0)[c] (0.0)[d]	(52.8)[a] (51.0)[b] (55.1)[c] (52.7)[d]	(0.0)[a] (0.0)[b] (0.0)[c] (0.0)[d]	(51.6)[a] (48.6)[b] (53.9)[c] (51.8)[d]	(0.0)[a] (0.0)[b] (0.0)[c] (0.0)[d]	(49.5)[a] (43.7)[b] (51.6)[c] (50.6)[d]

[a] From CCSD(T)/Def2-TZVPP [this work]. [b] From LC-ωPBE/Def2-TZVPP [this work].

[c] From B3LYP/Def2-TZVPP [this work]. [d] From MP2/Def2-TZVPP [this work][e] From HF/DZd, Ref. 15. [f]From MP2/6-31G(d,p), Ref. 18. [g] From XRD for (Cy-cAAC·)$_2$Si$_2$Cl$_4$, (Cy-cAAC = :C(CH$_2$)(CMe$_2$)(C$_6$H$_{10}$)N-2,6-*i*Pr$_2$C$_6$H$_3$), Ref 27. [c] From B3LYP/6-311+G(d), Ref. 26.

Table 3. B3LYP/Def2-TZVPP calculated energies (in hartree) of HOMO (ε_{HOMO}), LUMO (ε_{LUMO}), ε_{LUMO}-ε_{HOMO}, global hardness (η), global electronegativity (χ), $\Delta[\eta\ (C_{2h})$- $\eta\ (D_{2h})]$ and $\Delta[\chi\ (C_{2h})$- $\chi\ (D_{2h})]$ parameters for the *trans*-bent (C_{2h}) and planar (D_{2h}) configurations of compounds **1-4**.

compound	ε_{HOMO}	ε_{LUMO}	ε_{LUMO} - ε_{HOMO}	I	A	η	χ	$\Delta[\eta$ (C2h)-η (D2h)]	$\Delta[\chi\ (C_{2h})$- $\chi\ (D_{2h})]$
1, C_{2h}	-0.26688	-0.13092	0.13596	0.26688	0.13092	0.06798	0.19890	0.00418 (2.62)[a]	0.04968 (31.2)[a]
1, D_{2h}	-0.21302	-0.08542	0.12760	0.21302	0.08542	0.06380	0.14922	0.00000	0.00000
2, C_{2h}	-0.24729	-0.13928	0.10801	0.24729	0.13928	0.05400	0.19328	-0.00633 (-3.97)[a]	0.04536 (28.5)[a]
2, D_{2h}	-0.20827	-0.08760	0.12067	0.20827	0.08760	0.06033	0.14793	0.00000	0.00000
3, C_{2h}	-0.24397	-0.14313	0.10084	0.24397	0.14313	0.05042	0.19355	-0.00209 (-1.31)[a]	0.03824 (24.0)[a]
3, D_{2h}	-0.20783	-0.10280	0.10503	0.20783	0.10280	0.05251	0.15531	0.00000	0.00000
4, C_{2h}	-0.23314	-0.14181	0.09133	0.23314	0.14181	0.04566	0.18747	0.00165 (1.04)[a]	0.0282 (17.7)[a]
4, D_{2h}	-0.20323	-0.11521	0.08802	0.20323	0.11521	0.04401	0.15922	0.00000	0.00000

Table 4. NBO-B3LYP/Def2-TZVPP calculated stabilization energies (E_2, in kcal mol^{-1}) associated with the electron delocalizations, off-diagonal elements ($F_{ij,}$ in atomic unit), orbital energies (ε, in atomic unit), orbital occupancies (e), natural bond orders (*nbo*) and natural atomic charges (*NAC*) for the *trans*-bent (C_{2h}) geometries of compounds **1-4**.

compound	**1**	**2**	**3**	**4**
geometry	C_{2h}	C_{2h}	C_{2h}	C_{2h}
E_2				
$\pi_{si\text{-}si} \rightarrow \sigma^*_{si\text{-}si}$	72.76	29.65	25.16	19.78
Orbital occupancy				
$\pi_{Si\text{-}Si}$	1.607	1.782	1.791	1.812
$\sigma^*_{Si\text{-}Si}$	0.364	0.253	0.238	0.214
F_{ij}				
$\pi_{si\text{-}si} \rightarrow \sigma^*_{si\text{-}si}$	0.126	0.088	0.081	0.074
ε				
$\pi_{Si\text{-}Si}$	-0.22989	-0.27617	-0.28673	-0.29189
$\sigma^*_{Si\text{-}Si}$	0.04099	0.04475	0.03533	0.04680
$\Delta[\varepsilon(\sigma^*_{si\text{-}si}) - \varepsilon(\pi_{si\text{-}si})]$	0.27088	0.32092	0.32206	0.33869
Nbo				
Si-Si	1.281	1.470	1.487	1.531
Si-X	0.976	1.018	1.021	1.020
$\Delta[nbo(\text{Si-Si}) - nbo(\text{Si-X})]$	0.305	0.452	0.466	0.511
NAC				
Si	1.346	0.747	0.562	0.297
X	-0.673	-0.374	-0.281	-0.149
$\Delta[NAC\ (\text{Si}) - NAC\ (\text{X})]$	2.019	1.121	0.843	0.446

CCSD(T)/Def2-TZVPP

ΔE_o^a { **1**= 32.87; **2**= 16.32; **3**= 13.96; **4**= 10.25

LC-ωPBE/Def2-TZVPP

ΔE_o^a { **1**= 26.95; **2**= 8.56; **3**= 6.56; **4**= 3.87

LC-BLYP/Def2-TZVPP

ΔE_o^a { **1**= 30.11; **2**= 9.72; **3**= 7.61; **4**= 4.49

MP2/Def2-TZVPP

ΔE_o^a { **1**= 37.04; **2**= 14.56; **3**= 12.66; **4**= 10.00

B3LYP/Def2-TZVPP

ΔE_o^a { **1**= 36.62; **2**= 19.15; **3**= 17.35; **4**= 13.72

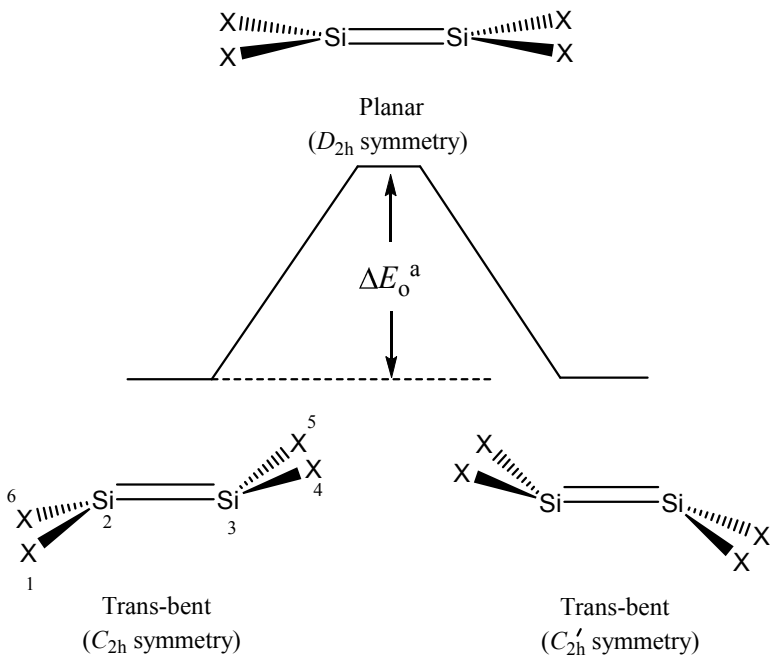

1: X=F, **2**: X=Cl, **3**: X=Br, **4**: X=I

Fig. 1. Calculated energy profiles of the *trans*-bent configurations interconversions of compounds **1-4** *via* their corresponding planar forms [$C_{2h} \rightarrow [D_{2h}]^{\neq} \rightarrow C_{2h}'$].

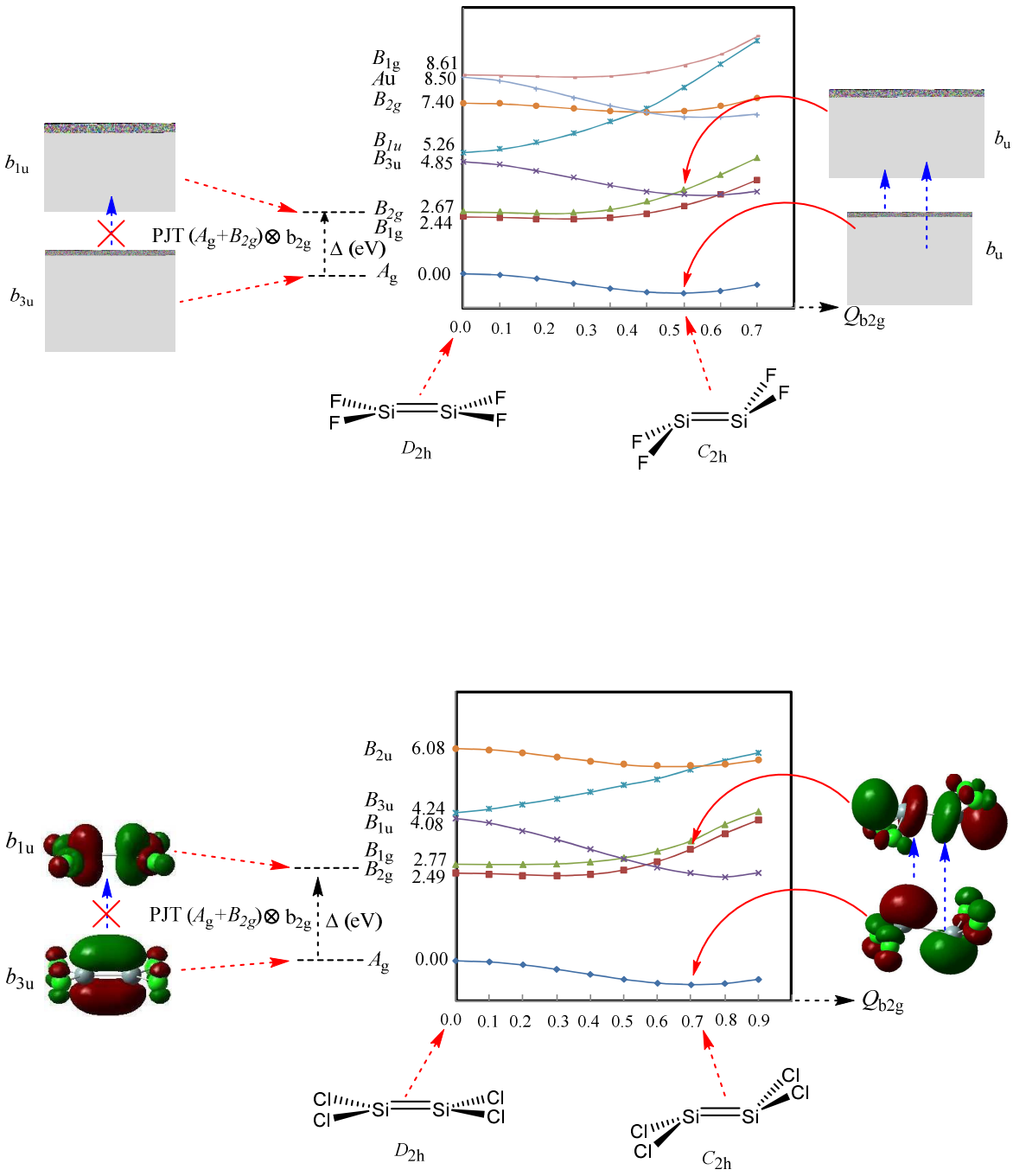

Fig. 2. TD-DFT (B3LYP/Def2-TZVPP) energy curves (in eV) of the ground and excited states in the bending directions of compounds **1-4**. At the planar structures [Q_{b2g} = 0.0], the symmetries of the electronic excited states (involved in the vibronic coupling) are B_{2g}.

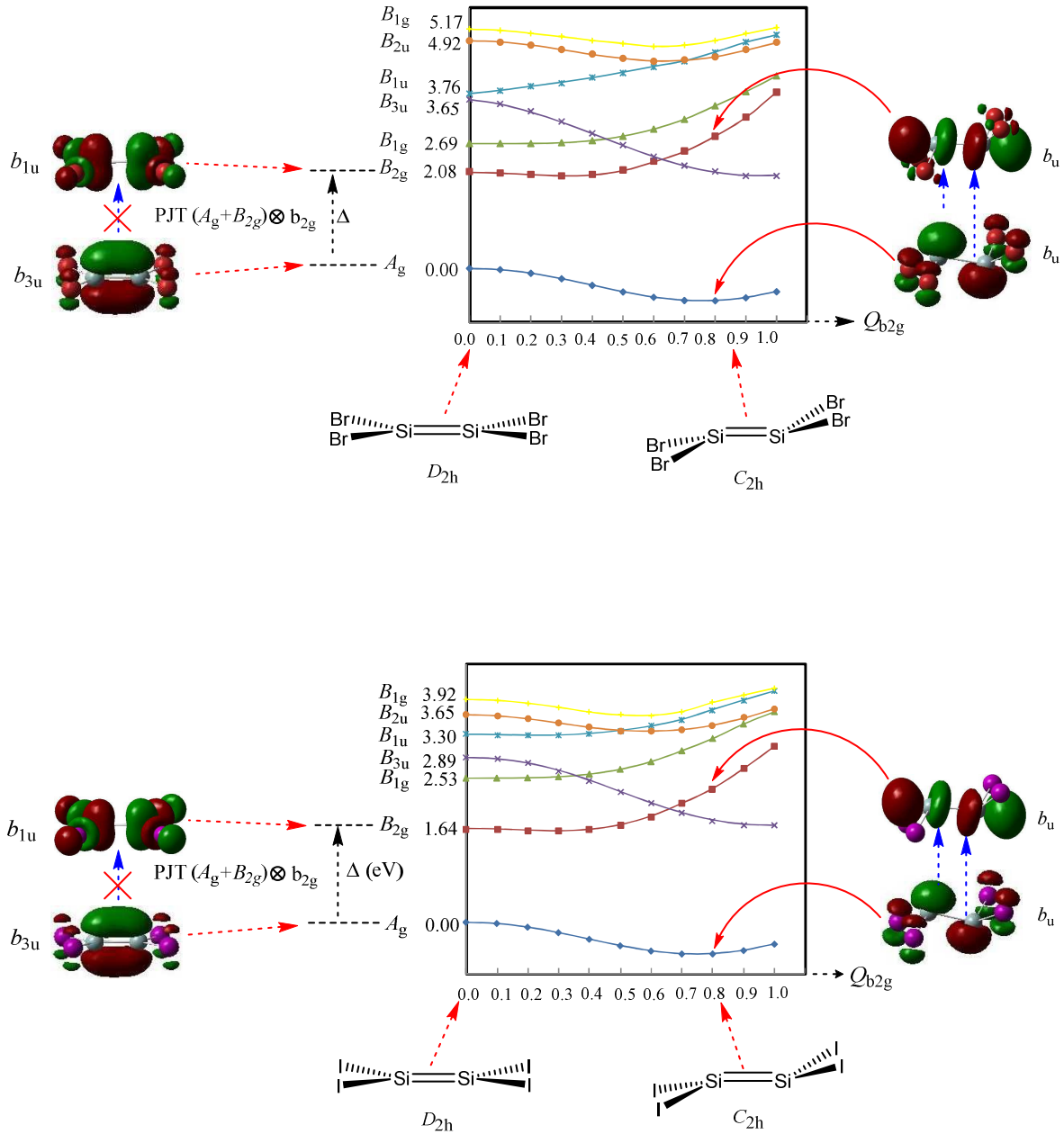

Fig. 2. Continued.

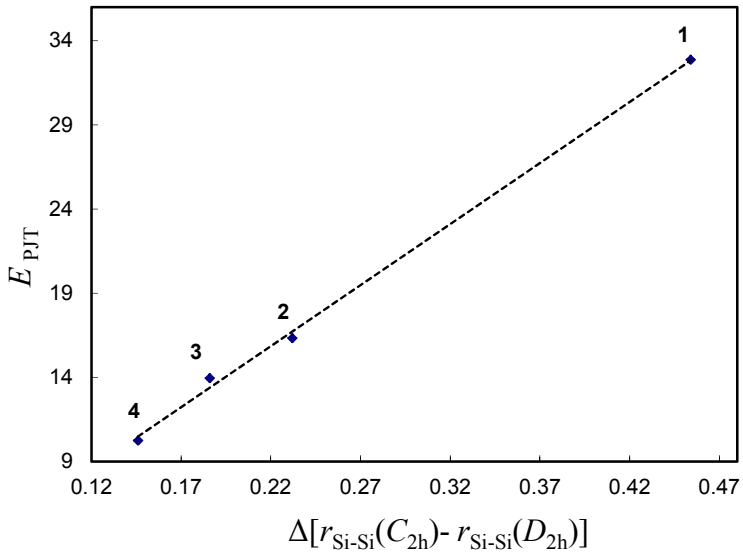

Figure 3. Fit of E_{PJT} versus $\Delta[r_{Si\text{-}Si}(C_{2h})\text{-}r_{Si\text{-}Si}(D_{2h})]$ parameters which shows a linear correlation represented by: E_{PJT} =72.607($\Delta[r_{Si\text{-}Si}(C_{2h})\text{-}\ r_{Si\text{-}Si}(D_{2h})]$)-0.1285 with R^2=0.9982.

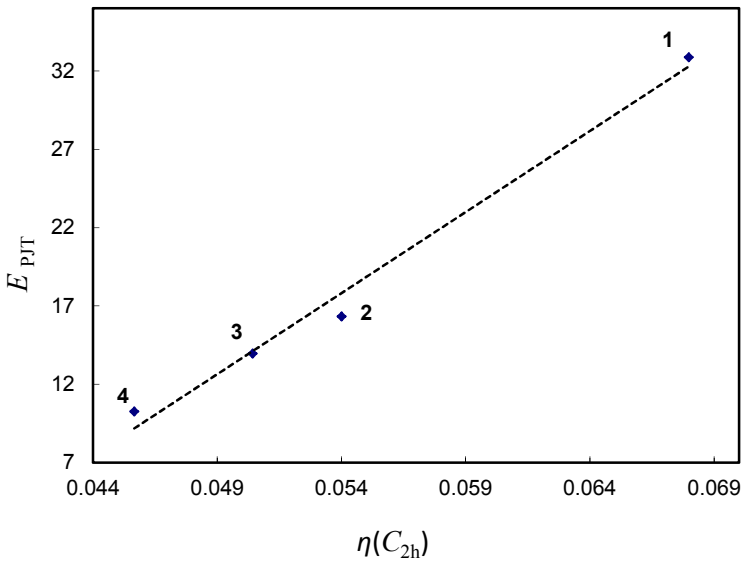

Figure 4. Fit of E_{PJT} versus the global hardness of the *trans*-bent (C_{2h}) structures [$\eta(C_{2h})$] of compounds **1-4** which shows a linear correlation represented by: E_{PJT} = 1034.4[$\eta(C_{2h})$] - 38.038, with R^2=0.9875.

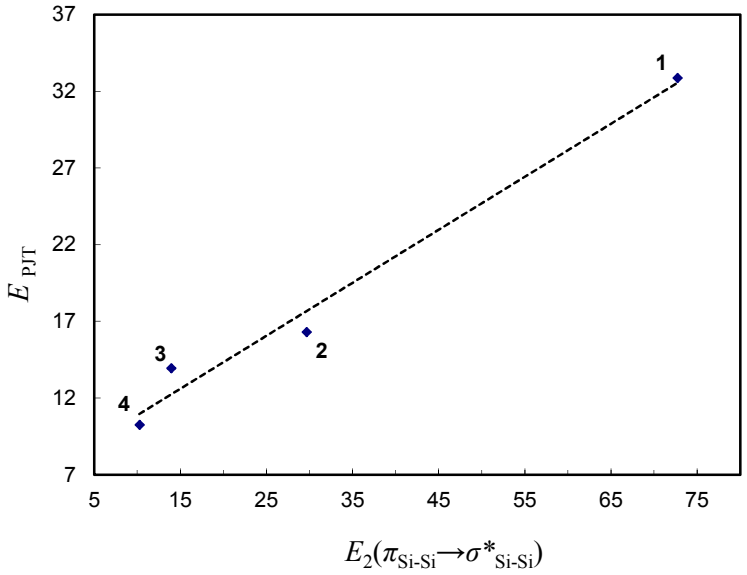

Figure 5. Fit of E_{PJT} versus the stabilization energies (E_2) associated with $\pi_{Si\text{-}Si} \rightarrow \sigma^*_{Si\text{-}Si}$ electron delocalizations which shows a linear correlation represented by: E_{PJT} = $0.3459[E_2(\pi_{Si\text{-}Si} \rightarrow \sigma^*_{Si\text{-}Si})]+ 7.4051$ with R^2=0.9821.

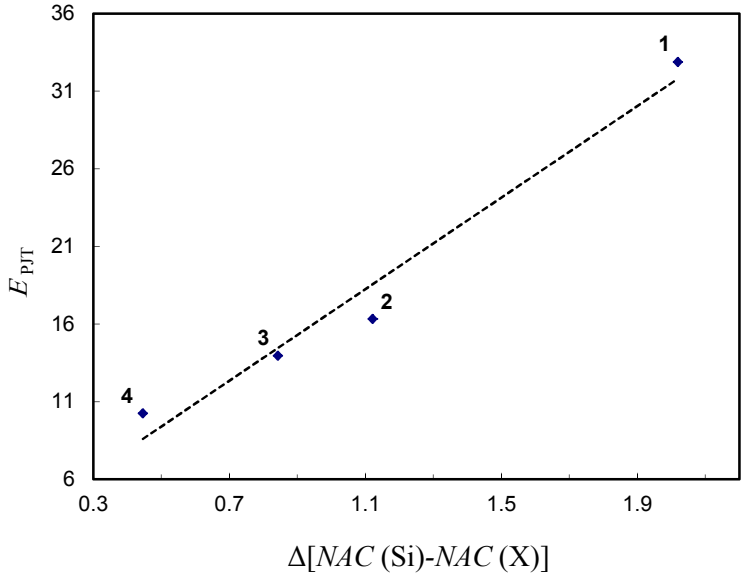

Figure 6. Fit of E_{PJT} versus the natural atomic charge (*NAC*) differences between the Si and halogen atoms (Δ[*NAC* (Si)-*NAC* (X)]) in the *trans*-bent (C_{2h}) structures of compounds **1-4** which shows a linear correlation represented by: E_{PJT} = $14.737(\Delta[NC\text{ (Si)-}NC\text{ (X)}] + 2.032$ $R^2 = 0.9696$.

Supplementary Information

Symmetry breaking in the planar configurations of disilicontetrahalides. Correlations between the Pseudo Jahn-Teller effect parameters, hardness and electronegativity

Ghazaleh Kouchakzadeh and Davood Nori-Shargh*

Table SI-1. LC-BLYP/Def2-TZVPP, LC-ωPBE/Def2-TZVPP and B3LYP/Def2-TZVPP calculated corrected electronic energies (E_o=E_{el}+*ZPE*) [zero point energies (*ZPE*) from B3LYP/Def2-TZVPP level] for the planar (D_{2h} symmetry) and bent (C_{2h} symmetry) geometries of compounds **1-4**.

Method	LC-BLYP/Def2-TZVPP			LC-ωPBE/Def2-TZVPP			B3LYP/Def2-TZVPP		
compound	*ZPE*	E_0	ΔE_0^a	*ZPE*	E_0	ΔE_0^a	*ZPE*	E_0	ΔE_0^a
1, C_{2h}	0.010945	-977.720106	0.00	0.011243	-978.325617	0.00	0.011062	-978.789737	0.00
1, D_{2h}	0.013279	-977.672125	30.11	0.012978	-978.282672	26.95	0.012652	-978.731386	36.62
2, C_{2h}	0.007894	-2418.519307	0.00	0.007967	-2419.291896	0.00	0.007288	-2420.099696	0.00
2, D_{2h}	0.008782	-2418.503821	9.72	0.008707	-2419.278261	8.56	0.008152	-2420.069176	19.15
3, C_{2h}	0.006303	-10873.755558	0.00	0.006360	-10874.132689	0.00	0.005644	-10875.913622	0.00
3, D_{2h}	0.006971	-10873.743436	7.61	0.006902	-10874.122226	6.56	0.006350	-10875.885970	17.35
4, C_{2h}	0.005534	-1768.549434	0.00	0.005588	-1769.887986	0.00	0.004864	-1770.373083	0.00
4, D_{2h}	0.005878	-1768.542280	4.49	0.005848	-1769.881968	3.78	0.005336	-1770.351212	13.72

Table SI-2. Calculated structural parameters of the planar (D_{2h}) and *trans*-bent (C_{2h}) geometries of compounds **1-4**.

Compound	**1**		**2**		**3**		**4**	
Geometry	D_{2h}	C_{2h}	D_{2h}	C_{2h}	D_{2h}	C_{2h}	D_{2h}	C_{2h}
Bond lengths (Å)								
$r_{si\text{-}si}$	(2.049)[a]	(2.844)[a]	(2.069)[a]	(2.329)[a]	(2.076))[a]	(2.290)[a]	(2.088)[a]	(2.227)[a]
	(2.064)[b]	(2.641)[b]	(2.083)[b]	(2.311)[b]	(2.090)[b]	(2.273)[b]	(2.101)[b]	(2.220)[b]
	(2.084)[c]	(2.638)[c]	(2.113)[c]	(2.426)[c]	(2.123)[c]	(2.404)[c]	(2.140)[c]	(2.365)[c]
	(2.048)[d]			(2.343)[e]				
$r_{si\text{-}x}$	(1.570)[a]	(1.588)[a]	(2.006)[a]	(2.035)[a]	(2.164)[a]	(2.194)[a]	(2.381)[a]	(2.409)[a]
	(1.581)[b]	(1.598)[b]	(2.012)[b]	(2.038)[b]	(2.170)[b]	(2.197)[b]	(2.385)[b]	(2.409)[b]
	(1.584)[c]	(1.604)[c]	(2.036)[c]	(2.076)[c]	(2.204)[c]	(2.249)[c]	(2.429)[c]	(2.477)[c]
	(1.591)[d]			(2.056)[e]				
$\Delta[r_{si\text{-}si}(C_{2h}) - r_{si\text{-}si}(D_{2h})]$[a]	0.795		0.260		0.214		0.139	
$\Delta[r_{si\text{-}si}(C_{2h}) - r_{si\text{-}si}(D_{2h})]$[b]	0.577		0.228		0.183		0.119	
$\Delta[r_{si\text{-}si}(C_{2h}) - r_{si\text{-}si}(D_{2h})]$[c]	0.554		0.313		0.281		0.225	
Bond angles (°)								
$\theta_{x\text{-}si\text{-}si}$	(125.5)[a]	(105.5)[a]	(123.6)[a]	(111.6)[a]	(122.8)[a]	(112.3)[a]	(121.8)[a]	(113.9)[a]
	(125.3)[b]	(106.6)[b]	(123.2)[b]	(112.1)[b]	(122.7)[b]	(112.8)[b]	(121.7)[b]	(114.2)[b]
	(125.1)[c]	(106.7)[c]	(123.0)[c]	(110.2)[c]	(122.5)[c]	(110.4)[c]	(121.7)[c]	(111.1)[c]
$\theta_{x\text{-}si\text{-}x}$	(109.1)[a]	(101.3)[a]	(113.3)[a]	(106.1)[a]	(114.4)[a]	(107.6)[a]	(116.3)[a]	(110.4)[a]
	(109.5)[b]	(102.3)[b]	(113.5)[b]	(106.8)[b]	(114.6)[b]	(108.2)[b]	(116.6)[b]	(110.9)[b]
	(109.8)[c]	(102.8)[c]	(114.0)[c]	(106.1)[c]	(115.1)[c]	(107.3)[c]	(116.7)[c]	(109.0)[c]
	(109.7)[d]							
Torsion angles (°)								
$\theta_{x\text{-}si\text{-}si\text{-}x}$	(0.0)[a]	(73.3)[a]	(0.0)[a]	(61.5)[a]	(0.0)[a]	(58.6)[a]	(0.0)[a]	(52.2)[a]
	(0.0)[b]	(71.3)[b]	(0.0)[b]	(60.0)[b]	(0.0)[b]	(57.0)[b]	(0.0)[b]	(50.8)[b]
	(0.0)[c]	(70.5)[c]	(0.0)[c]	(63.3)[c]	(0.0)[c]	(61.5)[c]	(0.0)[c]	(58.4)[c]
Flap Angles (°)								
	(0.0)[a]	(65.1)[a]	(0.0)[a]	(52.3)[a]	(0.0)[a]	(50.0)[a]	(0.0)[a]	(44.8)[a]
	(0.0)[b]	(62.9)[b]	(0.0)[b]	(51.0)[b]	(0.0)[b]	(48.6)[b]	(0.0)[b]	(43.7)[b]
	(0.0)[c]	(62.4)[c]	(0.0)[c]	(55.1)[c]	(0.0)[c]	(53.9)[c]	(0.0)[c]	(51.6)[c]

[a] From LC-BLYP/Def2-TZVPP [this work]. [b] From LC-wPBE/Def2-TZVPP [this work]. [c] From B3LYP/Def2-TZVPP [this work]. [d] From HF/DZd, see Ref. 15**.** [e]From MP2/6-31G(d,p), see Ref. 18.

Table SI-3. LC-ωPBE/Def2-TZVPP calculated energies (in hartree) of HOMO (ε_{HOMO}), LUMO (ε_{LUMO}), ε_{LUMO}-ε_{HOMO}, global hardness (η), global electronegativity (χ), $\Delta[\eta(C_{2h})$-$\eta(D_{2h})]$ and $\Delta[\chi(C_{2h})$-$\chi(D_{2h})]$ parameters for the *trans*-bent (C_{2h}) and planar (D_{2h}) configurations of compounds **1-4**.

compound	ε_{HOMO}	ε_{LUMO}	ε_{LUMO} - ε_{HOMO}	I	A	η	χ	$\Delta[\eta(C_{2h})$-$\eta(D_{2h})]$	$\Delta[\chi(C_{2h})$-$\chi(D_{2h})]$
1, C_{2h}	-0.35420	-0.05145	0.30275	0.35420	0.05145	0.15137	0.20282	-0.01082(-6.79)[a]	0.05645 (35.4)[a]
1, D_{2h}	-0.30856	0.01582	0.32438	0.30856	-0.01582	0.16219	0.14637	0.00000	0.00000
2, C_{2h}	-0.32112	-0.05677	0.26435	0.32112	0.05677	0.13217	0.18894	-0.02697(-16.92)[a]	0.04916 (30.8)[a]
2, D_{2h}	-0.29892	0.01936	0.31828	0.29892	-0.01936	0.15914	0.13978	0.00000	0.00000
3, C_{2h}	-0.31539	-0.06006	0.25533	0.31539	0.06006	0.12766	0.18772	-0.02132 (-13.38)[a]	0.03994 (25.1)[a]
3, D_{2h}	-0.29676	0.00120	0.29796	0.29676	-0.00120	0.14898	0.14778	0.00000	0.00000
4, C_{2h}	-0.30234	-0.05751	0.24483	0.30234	0.05751	0.12241	0.12241	-0.01364(-8.56)[a]	0.03093(19.4)[a]
4, D_{2h}	-0.28939	-0.01729	0.27210	0.28939	0.01729	0.13605	0.15334	0.00000	0.00000

Table SI-4. LC-BLYP/Def2-TZVPP calculated energies (in hartree) of HOMO (ε_{HOMO}), LUMO (ε_{LUMO}), ε_{LUMO}-ε_{HOMO}, global hardness (η), global electronegativity (χ), $\Delta[\eta(C_{2h})$-$\eta(D_{2h})]$ and $\Delta[\chi(C_{2h})$-$\chi(D_{2h})]$ parameters for the *trans*-bent (C_{2h}) and planar (D_{2h}) configurations of compounds **1-4**.

compound	ε_{HOMO}	ε_{LUMO}	ε_{LUMO} - ε_{HOMO}	I	A	η	χ	$\Delta[\eta(C2h)$-$\eta(D2h)]$	$\Delta[\chi(C_{2h})$-$\chi(D_{2h})]$
1, C_{2h}	-0.36963	-0.04456	0.32507	0.36963	0.04456	0.16254	0.20709	-0.00259(-1.63)[a]	0.06065 (38.1)[a]
1, D_{2h}	-0.31156	0.01869	0.33025	0.31156	-0.01869	0.16513	0.14644	0.00000	0.00000
2, C_{2h}	-0.32517	-0.05638	0.26879	0.32517	0.05638	0.13439	0.19077	-0.02867(-17.99)[a]	0.0532 (33.4)[a]
2, D_{2h}	-0.30062	0.02549	0.32611	0.30062	-0.02549	0.16306	0.13757	0.00000	0.00000
3, C_{2h}	-0.31961	-0.06074	0.25887	0.31961	0.06074	0.12943	0.19017	-0.02258 (-14.17)[a]	0.04319 (27.1)[a]
3, D_{2h}	-0.29899	0.00503	0.30402	0.29899	-0.00503	0.15201	0.14698	0.00000	0.00000
4, C_{2h}	-0.30536	-0.05736	0.24800	0.30536	0.05736	0.12400	0.18136	-0.01372 (-8.61)[a]	0.0278(17.4)[a]
4, D_{2h}	-0.29128	-0.01585	0.27543	0.29128	0.01585	0.13772	0.15357	0.00000	0.00000